PalArch's Journal of Archaeology of Egypt / Egyptology

SYNTHESIS OF FILLED SKUTTERUDITE COMPOUND $YB_xCO_4SB_{12}$ BY SOLID STATE MICROWAVE

Hussein Ghafel AL-Toki*[1], M. K. Salman*[2]

Microelectronics and Nanotechnology Research Laboratory (M. N. R. Lab.), Physics Department.

***[1] National University of Science and Technology, College of Pharmacy.**

***[2] College of petroleum engineering, University of Sumer.**

Hussein Ghafel AL-Toki, M. K. Salman, Synthesis of Filled Skutterudite Compound $Yb_xco_4sb_{12}$ by Solid State Microwave, Palarch's Journal of Archaeology of Egypt/Egyptology 18(8). ISSN 1567-214x.

Keywords: Skutterudite semiconductor, $Yb_xCo_4Sb_{12}$, thermoelectricmaterials, thermoelectric properties, X-ray diffraction

Abstract

The skutterudite semiconductor thermoelectric alloy $Yb_xCo_4Sb_{12}$ (x = *0.15*- 0.3) was synthesized by solid-state microwave. The morphology of the micro/nanostructure and polycrystalline stoichiometric ratio of $Yb_xCo_4Sb_{12}$ (x =*0.15*- 0.3) were examined using scanning electron microcopy (SEM) and energy dispersive X-ray spectra (EDX). The structures of the skutterudite polycrystalline alloy $Yb_xCo_4Sb_{12}$ were examined by X-ray diffraction (XRD) patterns. A cubic structure was observed, and the lattice constant increased with increasing amount of Yb, with doping levels from x=0.15 to 0.3 and saturated with increments. The thermoelectric properties including electrical conductivity (σ), Seebeck coefficient (α) and electrical power factor(PF) were measured at a temperature range of 298–

700 K. The transport properties of skutterudites alloy demonstrate a semiconductor behavior, during the temperature measurement, which indicated the change of electronic band structure. The Hall effect and Seebeck coefficient measurements have shown p-type conductivity in samples. The highest value of the Seebeck coefficient was 176.84 μV/K with doping levels x=0.3, at 329 K.

Keywords: Skutterudite semiconductor, $Yb_xCo_4Sb_{12}$, thermoelectric materials, thermoelectric properties, X-ray diffraction.

1. Introduction

Thermoelectric materials can be utilized for solid state power generation in a variety of applications, including automotive power generation and solar energy capture [1-3], they can directly convert thermal energy into electrical energy or vice versa [4]. Recently, filled skutterudites ($Yb_xCo_4Sb_{12}$) are known to be one of the state of the art materials for high temperature applications due to their high figure of merit $ZT = \alpha^2\sigma T/\lambda = \alpha^2 T/\rho(\lambda_L + \lambda_e)$, where α is the Seebeck coefficient (*i.e.*, thermo power), σ and ρ are electrical conductivity, electrical resistivity, respectively, λ the thermal conductivity (including the lattice thermal conductivity, λ_L, and the carrier thermal conductivity, λ_e), and *T* the absolute temperature in Kelvin [5-7] .The fact is the σ and α change in opposite directions with elemental doping, (α^2/ρ) is defined as the thermoelectric power factor (PF) to achieve a high-efficiency of thermoelectric material should be the thermal conductivity minimized and maximized of the power factor. Optimization PF is an important parameters such as effective mass, band gaps and crystal structure are also crucial [8]. Empty skutterudite compounds structure is composed of a cubic lattice with the space group *Im3*. Unfilled skutterudites are binary compounds of the form AX_3 (A = Co, Ir and Rh, X = Sb, P and As) , where A and X are transition metals and pnictogens, respectively [7, 9]. Skutterudite attracted great attention recently as new thermoelectric materials [10], because they possess high electrical conductivity, carrier mobility and relatively large Seebeck coefficients which give rise to a good ZT [11, 12], it have high thermal conductivity which make it difficult to be an efficient thermoelectric material [13]. Minimize the thermal conductivity, is found by using these techniques such as doping [14], nanostructuring [13, 15], nanoparticle dispersion of $CoSb_3$ [16, 17] have been developed, and rare earth metal filling [18, 19]. The doped of $CoSb_3$ with another rare earth element-ytterbium (Yb) a typical divalent metal with ground state and has two electrons in 5s shell the change of the Yb valence the maximum of the

electrons (14) in the 4*f* shell in Yb^{+2} ($4f^{14}5d^{0}6s^{2}$) to 13 electrons in Yb^{+3} state ($4f^{13}5d^{1}6s^{2}$), the position of the pinned Fermi level for $CoSb_3$ doped is defined by the balance between Yb^{+2} and Yb^{+3} charge states of the dopant [20]. The source of ionization are at $4f^{14}6s^{2}(^{1}S_{0})$ of Yb. Microwave irradiation is technique to synthesis and variety of compounds, where chemical reactions are accelerated because of selective absorption of microwaves by polar molecules [21]. Solid state microwave synthesis was recently demonstrated to be a fast, simple, energy efficient, and environmentally friendly technique. It radiations (2.45 GHz) polarized, coherent, and capable on coupling with atomic materials, resulting in the rapid heating of such materials [22]. The samples were examined by powder X-ray diffraction. The fine structure of the materials was studied using scanning electron microscopy (SEM). The electric conductivity and Seebeck coefficient were measured simultaneously by the standard four-probe method.

2. Experimental

In the present study, solid-state microwave synthesis was used to prepare the ternary polycrystalline ingots of $Yb_xCo_4Sb_{12}$. High purity elemental (99.999%), for the Yb, Co and Sb powders, were weighed using an electronic balance, in the present research to produce 2 g samples of (x= 0.15 and 0.3) ingots using the solid-state microwave synthesis. All elements were mixed, ground for 20 min using a mortar and pestle, and then placed inside a 10 mm (O.D.) × 8 mm (I.D.) quartz ampoule and sealed under a vacuum of 5×10^{-5} mbar. The samples were irradiated in an 1000 W (100% power) MG 1443ARW microwave (LG) at 2.45 GHz for 10 min. Bright whitish blue plasma was observed emerging from two ampoules from the first minute of microwave exposure. The temperature of the samples was measured using an OS524E infrared thermometer (OMEGA SCOPE) with values ranging from 1173 to 1183 K. After microwave irradiation subsequently, $Yb_xCo_4Sb_{12}$ (x=0.15-0.3) powders were pressed into disk shapes (diameter: 12 mm; thickness: 0.71 mm) via cold pressing at 10 tons. The Seebeck coefficient (α) was determined by the slope of the linear relationship between the thermo electromotive force and the temperature difference between the two ends of each sample. The electrical conductivity (σ) was measured using the four point probe dc method under a vacuum of 10^{-3} mbar within temperatures ranging from room temperature to about 700 K. The Hall coefficient (R_H) was determined at room temperature with an applied magnetic field of 1 T using a PHYWE electromagnetic power supply (model: 305D).

3. Results and discussion

3.1 SEM and EDX analyses of $Yb_xCo_4Sb_{12}$ disks

Fig.1 displays a typical SEM and EDX images of the surface morphology and elemental compositions of the $Yb_xCo_4Sb_{12}$ ingots prepared through solid state microwave synthesis. Typical SEM images of the surface morphology of the resultant disks the average grain size about 500 nm of sample, which is probably due to the grain growth from the alloyed portion of the powders during the press process [13]. The clear facets show that the grains are well crystallized. The SEM image also shows that the crystallized grains are closely packed. To determine the elemental compositions of the $Yb_xCo_4Sb_{12}$ the stoichiometric ratio of the structure based on the EDX composition analysis, Fig.1 was used to investigate the Yb-doping ratio. According to these EDX spectra, the incorporated elements can be estimated, the amount of Yb substituted for stoichiometric ratio of the ingots samples. The samples Yb contents gradually increased from x = 0.15 - 0.3. Table 1 shows the actual weight and atomic percentage of every element in the $Yb_xCo_4Sb_{12}$ disk.

3.2 X-ray diffraction (XRD) analysis of $Yb_xCo_4Sb_{12}$ powders

The XRD patterns within a scan range of 20° to 80° for $Yb_xCo_4Sb_{12}$ powders with different Yb contents (x=0.15 – 0.3). XRD patterns were obtained to determine the crystalline quality of the compounds. Fig. 2 show the patterns indicated that these substances were polycrystalline and characterized by has cubic structure. Where positions all diffraction peak of the Miller indices (*hkl*) fully matched with values obtained from the standard JCPDS file No19-0336 and well matched with reported data were the lattice parameter 9.057 Å of the Zhen Xiong et. al. [23-25]. The cubic lattice constant of the binary and ternary compounds can be calculated from the XRD data [26] as show in Table 2.

3.3 Electrical conductivity of $Yb_xCo_4Sb_{12}$ disks

The electrical conductivity (σ) values of samples prepared by solid state microwave synthesis were measured by home built equipment using the Van der Pauw method. Fig. 3 shows the relationship between σ and temperature ranging from 298 K to 700 K for the

$Yb_xCo_4Sb_{12}$ disks. σ increases with temperature increase, in all specimens, representing non-degenerate semiconductors conducting behavior, this result agreement with Gaosheng Fu,et. al. [27], with its values decreased from 4.354×10^3 *S/m to* 1.046×10^3 *S/m* at 300 K and from 1.624×10^4 *S/m* to 7.648×10^3 *S/m* at 686 K with increased Yb content from x= 0.15 -0.30 , respectively. This behavior might be because of the increase charge carrier concentration, this is consistent with the result reported by Mohammed Amin [28]. To estimate both the Hall coefficient (R_H), holes concentration (p) and mobility (μ_h) of the samples were determined from the Hall effect measurements as displayed in the Table 3.

3.4 Seebeck coefficient of $Yb_xCo_4Sb_{12}$ disks

Fig. 4 Show the Seebeck coefficient (α) terms of the measured temperature for the $Yb_xCo_4Sb_{12}$ is all the specimens had a positive value (p-type), suggesting that the holes were demonstrate that the majority of charge carriers within the measured temperature range. This finding agreed with the results of Hall effect results listed in Table 4. α value change with increase in Yb content, that a high holes concentration yields a value low of α and high σ [29]. In single-phase doped skutterudites, the absolute α decrease with the hole concentration increase [30]. Consider the increase of the α is mainly caused by potential barrier scattering, they should form in grain boundaries when the grain size is small, carriers with high energy will overcome the potential barrier, while the lower energy will be strongly scattered or stopped by the potential barrier at grain boundaries [31]. The highest value for α was 368 μV/K at 305 K for $Yb_{0.3}Co_4Sb_{12}$ as Fig. 4. The doping with rare-earth element ytterbium the position of the pinned Fermi level is defined by the balance between Yb^{2+} and Yb^{3+} charge states of the dopant [20, 32]. Yb typical divalent metal with ground state and has two electrons in 5*s* the change of the Yb valence the maximum of the electrons (14) in the 4*f* shell in Yb^{+2} ($4f^{14}5d^06s^2$) to 13 electrons in Yb^{+3} state ($4f^{13}5d^16s^2$), the source of ionization are at $4f^{14}6s^2(^1S_0)$ of Yb [20]. The electron paramagnetic resonance is shown in the case of doped Yb, Fermi-level pinning is provided by switching the impurity valence by one: Yb^{2+}–Yb^{3+}. The electron from the Yb^+ state may transfer to the conduction band, then usually the Fermi level is pinned near the top of the valence band and the samples is of the p-type, these results can be compared with literature for PbTe doped with Yb [20, 28, 32].

3.5 Power factor of $Yb_xCo_4Sb_{12}$ disks

The power factor ($\alpha^2\sigma$) of $Yb_xCo_4Sb_{12}$ was calculated from σ and α. The relationship of the measured temperature with $\alpha^2\sigma$ for the $Yb_xCo_4Sb_{12}$ is showing in Fig. 5. $\alpha^2\sigma$ was calculated based on the measured α and σ, which strongly increase at the room temperature because σ exhibits intrinsic conduction caused by the increase of hole carriers [33, 34]. The highest $\alpha^2\sigma$ calculated at 300 K for the $Yb_{0.30}Co_4Sb_{12}$ sample had a maximum value is 141.673 μW/mK^2. This result can be ascribed the is mainly due to the enhancement of electrical conductivity [35], as show in the Table 4.

4. Conclusions

This study reports the polycrystalline synthesis of cubic structure for Yb_xCo4Sb_{12} composition at mole fractions ranging from (x=0.15-0.30). Successfully merged polycrystalline ingots of Yb_xCo4Sb_{12} by solid state microwave synthesis technique. In addition, the behavior of Yb-doping with increased lattice constant of the powder. The measurements of the electrical properties showed that the samples were non-degenerate p-type semiconductors, were measured from ambient temperature of up to 700 K. The electrical conductivity decreases with the increase of Yb-doping of the rates (x=0.15-0.3). The maximum value for α was 368 μV/K at 305K for $Yb_{0.30}Co_4Sb_{12}$. The highest power factor calculated at 300 K for the $Yb_{0.30}Co_4Sb_{12}$ sample had a maximum value at 141.673 μW/mK^2.

Acknowledgments

The authors are grateful for the Microelectronics and Nanotechnology Research Laboratory (M. N. R. Lab.), Physics Department, College of Science, University of Basrah, for the help extended the research.

Figure captions

Fig.1 SEM and EDX images of $Yb_xCo_4Sb_{12}$ ternary disks for x=0.0, 0.15, 0.3, 0.45, 0.6, and 0.75.

Fig. 2 XRD patterns of the $Yb_xCo_4Sb_{12}$ powders prepared by solid state microwave synthesis, where (x=0.0-0.75).

Fig. 3 Electrical conductivities versus the temperature of the $Yb_xCo_4Sb_{12}$ disks.

Fig. 4 Seebeck coefficient versus temperature of $Yb_xCo_4Sb_{12}$ disks.

Fig. 5 Power factor versus the temperature of the $Yb_xCo_4Sb_{12}$ disks.

Table captions

Table 1: EDX elemental composition results of $Yb_xCo_4Sb_{12}$ disks with different Yb content.

Table 2: The structural properties: lattice constant (a), diffraction peak (2θ) and inter-planer distance (d) of $Yb_xCo_4Sb_{12}$ powders with different Yb content.

Table 3: The Hall coefficient (R_H), holes concentration (p) and carrier motilities (μ_H) of the $Yb_xCo_4Sb_{12}$.

Table 4: The Seebeck coefficient (α) and power factor ($\alpha^2\sigma$) of the $Yb_xCo_4Sb_{12}$ with different Yb composition at 300K.

References

[1] Bell, L.E., Cooling, heating, generating power, and recovering waste heat with thermoelectric systems. Science, 2008. 321(5895): p. 1457-1461.

[2] Yang, J. Potential applications of thermoelectric waste heat recovery in the automotive industry. in Thermoelectrics, 2005. ICT 2005. 24th International Conference on. 2005. IEEE.

[3] Tritt, T.M., H. Böttner, and L. Chen, Thermoelectrics: Direct solar thermal energy conversion. MRS bulletin, 2008. 33(04): p. 366-368.

[4] DiSalvo, F.J., Thermoelectric cooling and power generation. Science, 1999. 285(5428): p. 703-706.

[5] Tritt, T.M. and M. Subramanian, Thermoelectric materials, phenomena, and applications: a bird's eye view. MRS bulletin, 2006. 31(03): p. 188-198.

[6] Tritt, T.M., Thermoelectric phenomena, materials, and applications. Annual review of materials research, 2011. 41: p. 433-448.

[7] Nolas, G., D. Morelli, and T.M. Tritt, Skutterudites: A phonon-glass-electron crystal approach to advanced thermoelectric energy conversion applications. Annual Review of Materials Science, 1999. 29(1): p. 89-116.

[8] Hmood, A., A. Kadhim, and H.A. Hassan, Fabrication and characterization of $Pb_{1-x}Yb_xTe$ based alloy thin-film thermoelectric generators grown by thermal evaporation technique. Materials Science in Semiconductor Processing, 2013. 16(3): p. 612-618.

[9] Uher, C., Skutterudites: Prospective novel thermoelectrics. Semiconductors and semimetals, 2001. 69: p. 139-253.

[10] Fleurial, J., T. Caillat, and A. Borshchevsky. Skutterudites: an update. Thermoelectrics, 1997. in Proceedings ICT'97. XVI International Conference on. 2002.

[11] Chen, L., et al., Anomalous barium filling fraction and n-type thermoelectric performance of $Ba_yCo_4Sb_{12}$. Journal of Applied Physics, 2001. 90(4): p. 1864-1868.

[12] Sharp, J., et al., Thermoelectric properties of $CoSb_3$and related alloys. Journal of Applied Physics, 1995. 78(2): p. 1013-1018.

[13] Mi, J., et al., Nanostructuring and thermoelectric properties of bulk skutterudite compound $CoSb_3$. Journal of Applied Physics, 2007. 101(5): p. 054314.

[14] Chitroub, M., F. Besse, and H. Scherrer, Thermoelectric properties of semi-conducting compound $CoSb_3$doped with Pd and Te. Journal of Alloys and Compounds, 2009. 467(1): p. 31-34.

[15] Toprak, M.S., et al., The impact of nanostructuring on the thermal conductivity of thermoelectric $CoSb_3$. Advanced Functional Materials, 2004. 14(12): p. 1189-1196.

[16] Li, J., et al., Solvothermal synthesis of nano-sized skutterudite $Co_{4-x}Fe_xSb_{12}$ powders. Materials Chemistry and Physics, 2008. 112(1): p. 57-62.

[17] He, Z., et al., Nano $ZrO_2/CoSb_3$ composites with improved thermoelectric figure of merit. Nanotechnology, 2007. 18(23): p. 235602.

[18] Sales, B., D. Mandrus, and R.K. Williams, Filled skutterudite antimonides: a new class of thermoelectric materials. Science, 1996. 272(5266): p. 1325.

[19] Liu, K., X. Dong, and Z. Jiuxing, The effects of La on thermoelectric properties of $La_xCo_4Sb_{12}$ prepared by MA–SPS. Materials Chemistry and Physics, 2006. 96(2): p. 371-375.

[20] Ivanchik, I., et al., Giant negative magnetoresistance effect in PbTe (Yb, Mn). Physical Review B, 2000. 61(22): p. R14889.

[21] Hermkens, P.H., H.C. Ottenheijm, and D.C. Rees, Solid-phase organic reactions II: A review of the literature Nov 95–Nov 96. Tetrahedron, 1997. 53(16): p. 5643-5678.

[22] Suriwong, T., S. Thongtem, and T. Thongtem, Solid-state synthesis of cubic ZnTe nanocrystals using a microwave plasma. Materials Letters, 2009. 63(24): p. 2103-2106.

[23] Xiong, Z., et al., High thermoelectric performance of $Yb_{0.26}Co_4Sb_{12/y}GaSb$ nanocomposites originating from scattering electrons of low energy. Acta Materialia, 2010. 58(11): p. 3995-4002.

[24] He, T., et al., Thermoelectric properties of indium-filled skutterudites. Chemistry of materials, 2006. 18(3): p. 759-762.

[25] Takizawa, H., et al., Atom insertion into the $CoSb_3$ skutterudite host lattice under high pressure. Journal of Alloys and Compounds, 1999. 282(1-2): p. 79-83.

[26] Cullity, B.D., Elements of X-ray Diffraction. 2001.

[27] Fu, G., et al., Thermoelectric properties of DC-sputtered filled skutterudite thin film. Journal of Applied Physics, 2015. 117(12): p. 125304.

[28] Hossain, M.A., Fabrication and Characterization of Bulk Nanostructured Cobalt Antimonide based Skutterudites Materials for Thermoelectric Applications, 2015.

[29] Nolas, G.S., J. Poon, and M. Kanatzidis, Recent developments in bulk thermoelectric materials. MRS bulletin, 2006. 31(3): p. 199-205.

[30] Bai, S., et al., Enhanced thermoelectric performance of dual-element-filled skutterudites $Ba_xCe_yCo_4Sb_{12}$. Acta Materialia, 2009. 57(11): p. 3135-3139.

[31] Broido, D. and N. Mingo, Theory of the thermoelectric power factor in nanowire-composite matrix structures. Physical Review B, 2006. 74(19): p. 195325.

[32] Nikolić, P., et al., Far infrared properties of PbTe doped with cerium. Journal of Alloys and Compounds, 2007. 433(1-2): p. 292-295.

[33] Kadhim, A., A. Hmood, and H.A. Hassan, Chalcogen-based thermoelectric power generation device using p-type $Bi_{0.4}Sb_{1.6}Se_{2.4}Te_{0.6}$ and n-type $Bi_2Se_{0.6}Te_{2.4}$ prepared by solid-state microwave synthesis. Materials Science in Semiconductor Processing, 2013. 16(2): p. 537-541.

[34] Hmood, A., A. Kadhim, and H.A. Hassan, Structural and electrical properties of semimagnetic semiconductors $Pb_{1-x}Yb_xSe$ thin films. Superlattices and Microstructures, 2013. 53: p. 39-48.

[35] Yang, J., Thermoelectric Properties of $CoSb_3$-Based Skutterudites, 2010, Boston College. Graduate School of Arts and Sciences.

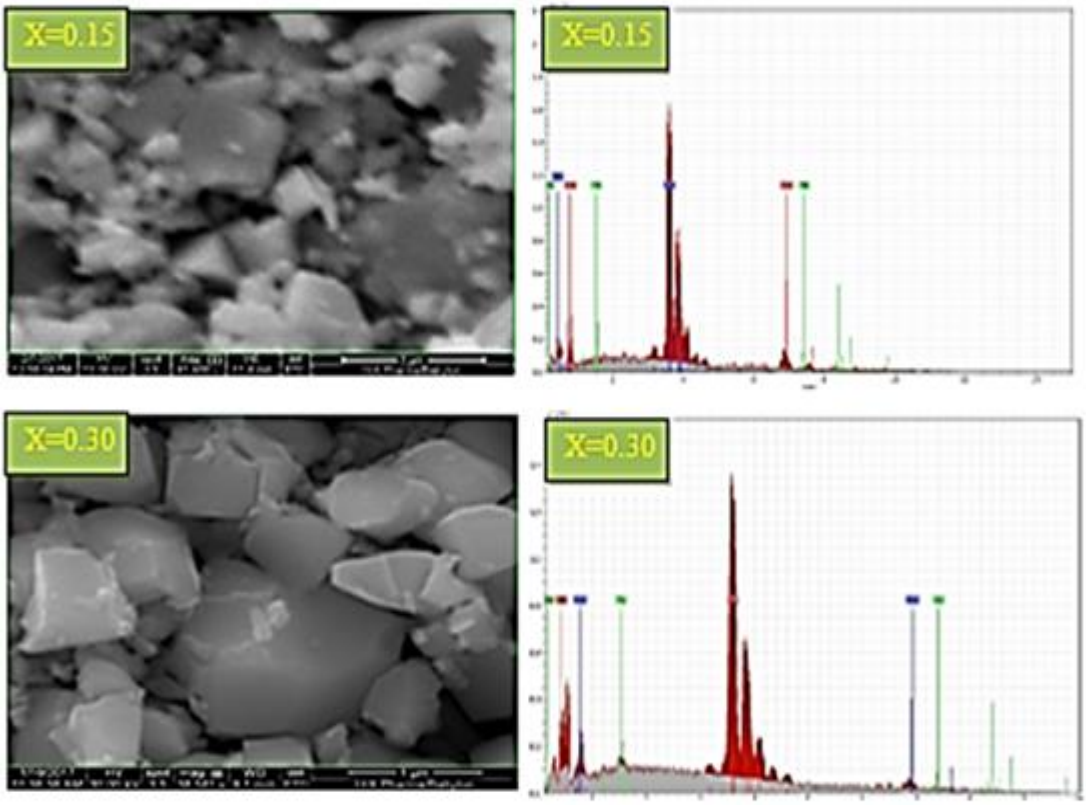

Fig.1 SEM and EDX images of $Yb_xCo_4Sb_{12}$ ternary disks for x= 0.15 and 0.3.

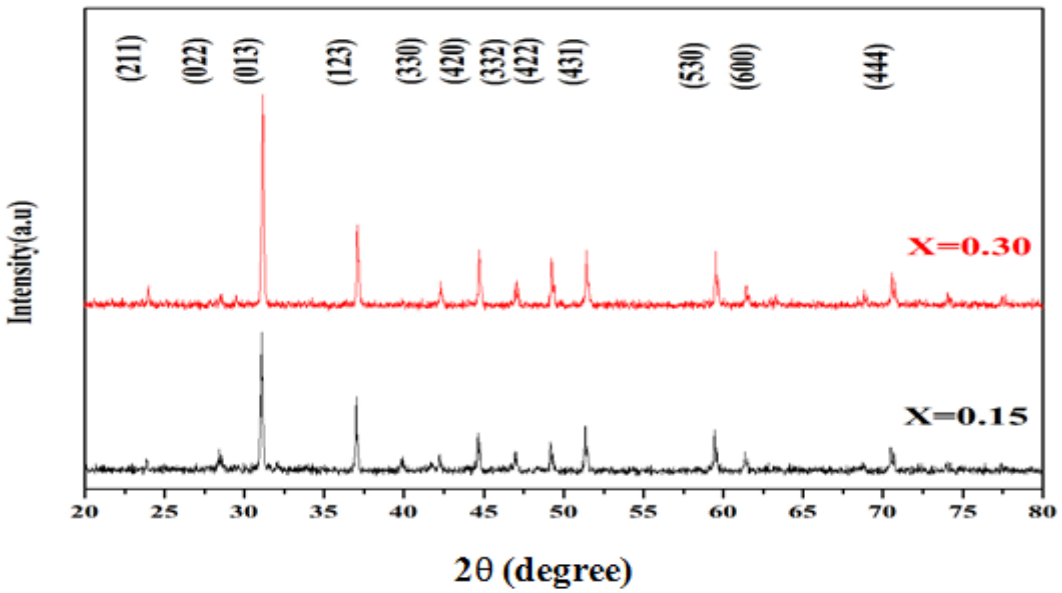

Fig. 2 XRD patterns of the $Yb_xCo_4Sb_{12}$ powders prepared by solid state microwave synthesis, where (x=0.15-0.30)

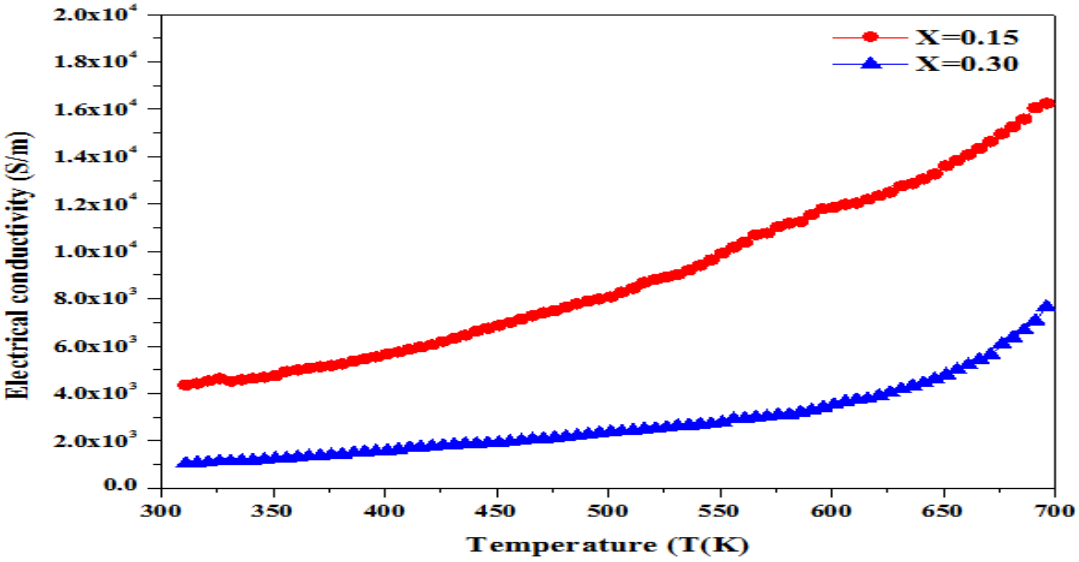

Fig. 3 The electrical conductivity versus the temperature of the $Yb_xCo_4Sb_{12}$ disks.

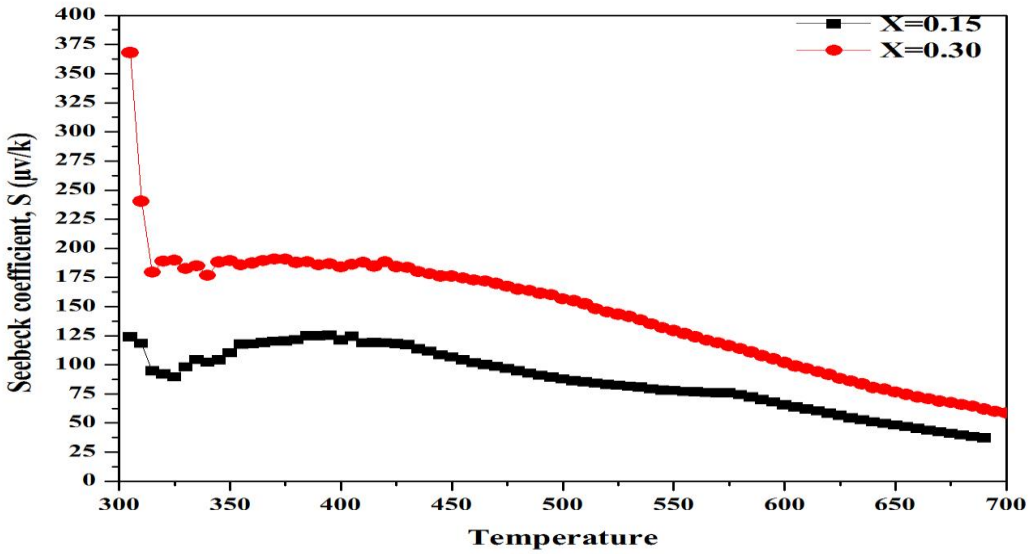

Fig.4 Seebeck coefficient versus temperature of $Yb_xCo_4Sb_{12}$.

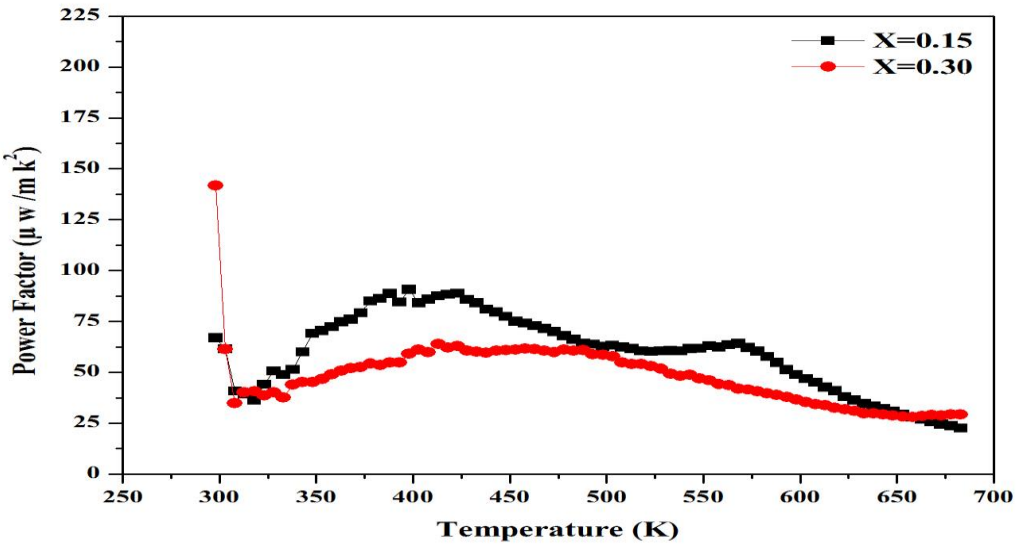

Fig. 5 Power factor versus the temperature of the $Yb_xCo_4Sb_{12}$

Table 1: EDX elemental composition results of $Yb_xCo_4Sb_{12}$ disks with different Yb content.

Sample	Element	Weight%	Atomic%
$Yb_{0.15}Co_4Sb_{12}$	Yb	0.74	0.97
	Co	13.31	13.27
	Sb	83.76	85.76
$Yb_{0.30}Co_4Sb_{12}$	Yb	1.44	1.70
	Co	9.60	7.71
	Sb	88.96	90.59

Table 2: The structural properties: lattice constant (*a*), diffraction peak (2θ) and inter-planer distance (d) of $Yb_xCo_4Sb_{12}$ powders with different Yb content.

Sample	Yb content	2θ	*d* (Å)	*a* (Å)
$Yb_{0.15}Co_4Sb_{12}$	0.15	31.069	2.878	9.101
$Yb_{0.3}Co_4Sb_{12}$	0.30	31.155	2.870	9.075

Table 3: The Hall coefficient (R_H), holes concentration (p) and carrier mobtilities (μ_H) of $Yb_xCo_4Sb_{12}$.

Sample	Yb content	$p*10^{18}$ (cm^{-3})	R_H (cm^3c^{-1})	μ_H ($cm^2v^{-1}s^{-1}$)
$Yb_{0.15}Co_4Sb_{12}$	0.15	0.146	42.717	2208.42
$Yb_{0.30}Co_4Sb_{12}$	0.30	0.030	202.33	2205.03

Table 4 The Seebeck coefficient and power factor of the $Yb_xCo_4Sb_{12}$ with different Yb composition at 300K.

Samples	Yb content	α (μV/K)	$\alpha^2\sigma$ (μW/mK^2)
$Yb_{0.15}Co_4Sb_{12}$	0.15	124	66.949
$Yb_{0.3}Co_4Sb_{12}$	0.30	368	141.673